Featured in Physics

Metasurface for Water-to-Air Sound Transmission

Eun Bok,[1] Jong Jin Park,[1] Haejin Choi,[1] Chung Kyu Han,[1] Oliver B. Wright,[2] and Sam H. Lee[1,*]
[1]Institute of Physics and Applied Physics, Yonsei University, Seoul 03722, Korea
[2]Faculty of Engineering, Division of Applied Physics, Hokkaido University, Sapporo 060-8628, Japan

(Received 24 August 2017; published 26 January 2018)

Effective transmission of sound from water to air is crucial for the enhancement of the detection sensitivity of underwater sound. However, only 0.1% of the acoustic energy is naturally transmitted at such a boundary. At audio frequencies, quarter-wave plates or multilayered antireflection coatings are too bulky for practical use for such enhancement. Here we present an acoustic metasurface of a thickness of only $\sim\lambda/100$, where λ is the wavelength in air, consisting of an array of meta-atoms that each contain a set of membranes and an air-filled cavity. We experimentally demonstrate that such a meta-atom increases the transmission of sound at ~700 Hz by 2 orders of magnitude, allowing about 30% of the incident acoustic power from water to be transmitted into air. Applications include underwater sonic sensing and communication.

DOI: 10.1103/PhysRevLett.120.044302

Impedance matching between two media has been extensively studied in relation to high fidelity acoustic devices [1–10]. However, the efficient transmission of sound from water to air has remained out of reach [11] owing to the huge ratio of 3600 in the acoustic impedances. With a conventional quarter-wavelength layer for acoustic impedance matching [7], one can optimally choose its acoustic impedance equal to the geometric mean of that of air and water. However, the required layer material, with an acoustic impedance ~60 times that of air, is not readily available. Moreover, at audio frequencies, such a layer is inconveniently bulky. Many studies on sound transmission at the water-air interface have been made, but there have been no realizations that have dramatically improved the performance of acoustic devices [11–15]. Effective water-to-air sound transmission would allow the use of air-based detectors such as capacitor-type microphones for underwater sound detection, which are generally about 3 orders of magnitude more sensitive than piezoelectric transducers [16]. High signal-to-noise detection of underwater sound is important in marine biology, sonar, underwater communication, and positioning systems. Good air-to-water transmission would allow the exploitation of the high efficiency of in-air loudspeakers for the emission of underwater audio-frequency acoustic waves.

One possible solution to this problem is the use of acoustic metamaterials [11,36–41], which provide significant advantages in the absorption, isolation, and transmission of sound. Acoustic metasurfaces are artificial two-dimensional (2D) structures containing resonator arrays for wave control, first proposed in the context of optics [42]. They consist of subwavelength-sized unit cells, or meta-atoms, in 2D, as opposed to general 3D acoustic metamaterials. Acoustic metasurfaces can form compact high-efficiency thin acoustic devices, such as lenses [43], mirrors [44], absorbers [45,46], or impedance matching units between two media [11,47,48]. However, as in the case of conventional acoustics, impedance matching in the extreme mismatch case has never been realized [11]. A clue to how to do this comes from the versatility of acoustic-metamaterial designs involving loaded membranes, useful for isolating sound [49–54]. Recently, hybrid resonances of loaded membranes have also been used to achieve extraordinary sound absorption [46,55–57] and acoustic energy harvesting [46], but the potential of loaded-membrane structures in sound transmission applications has not been explored so far.

In this Letter, we demonstrate that metasurfaces based on loaded membranes can provide effective sound transmission between media in the extreme mismatch case: we experimentally and theoretically demonstrate efficient water-to-air audio sound transmission with an ultrathin meta-atom of thickness $\ll\lambda$, where λ is the wavelength in air. Experiments and simulations are performed at a constant frequency, but the results are scalable, and arrays of our meta-atoms with different frequencies could be used to cover wide frequency ranges. We also investigate, by means of simulations described in the Supplemental Material [16], how an array of such meta-atoms can form an impedance matched metasurface. This work should open up entirely new avenues of acoustic communication to or from immersed sound sources.

We first describe the basic theory of our metasurface with a simplified lossless acoustic meta-atom before describing the fabricated meta-atom. Consider the case of air-to-water acoustic transmission. The acoustic wave equation obeys the principle of reciprocity, and so yields the same reflection and transmission coefficients as the water-to-air case [58,59]. Our effectively 1D system

consists of a tube, part of which is filled with water and part with air. We put a meta-atom at the air-water interface to achieve impedance matching in the same way as a localized meta-atom in a tube of air can achieve extraordinary acoustic transmission [60]. By elucidating the physics of a meta-atom, a metasurface can be understood. Our 1D cylindrical waveguide system with a bare air-water interface at the origin ($x = 0$) is shown in Fig. 1(a). For a "meta-atom" composed solely of air of thickness l, the power reflection coefficient R at a virtual interface $x = -l$ confronting a sinusoidal acoustic wave of wavelength λ incident in air is given by

$$R = \left| \frac{Z_l - Z_a}{Z_l + Z_a} \right|^2. \tag{1}$$

The impedance Z_a is given by $\rho_a c_a / S$, where $S(= \pi r^2)$ is the waveguide cross-sectional area, and ρ_a and c_a are, respectively, the density and the phase velocity of air. The acoustic impedance Z_l, defined as the pressure divided by the volume velocity at the virtual interface, is given by

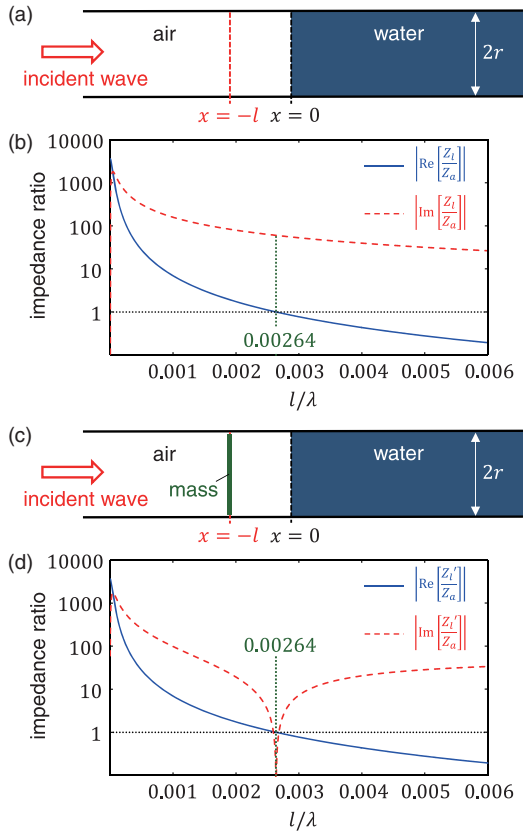

FIG. 1. (a) Subwavelength-diameter waveguide with a bare air-water interface, with acoustic incidence from the air side. (b) Analytically calculated absolute values of the real (solid blue line) and imaginary (dashed red line) parts of the normalized acoustic impedance Z_l at $x = -l$, plotted on a log-linear scale vs l/λ. (c) Case in which a sliding thin mass is placed at $x = -l$. (d) As in (b), but in the presence of the meta-atom.

$$Z_l = \frac{Z_w}{1 + (Z_w^2/Z_a^2 - 1)\sin^2(2\pi \frac{l}{\lambda})} - j\frac{Z_a}{2}\frac{(Z_w^2/Z_a^2 - 1)\sin(4\pi \frac{l}{\lambda})}{1 + (Z_w^2/Z_a^2 - 1)\sin^2(2\pi \frac{l}{\lambda})}, \tag{2}$$

where $Z_w = \rho_w c_w / S$ and ρ_w, c_w are the density and the phase velocity of water, respectively. This equation for the nondissipative case is a classical result [61], and indicates that the acoustic impedance changes as the virtual interface is moved away from the air-water interface owing to the presence of both incident and reflected waves. $\mathrm{Re}[Z_l]$ and $\mathrm{Im}[Z_l]$ are positive and negative, respectively; plots of $|\mathrm{Re}[Z_l/Z_a]|$ and $|\mathrm{Im}[Z_l/Z_a]|$ vs l/λ are shown in Fig. 1(b) on a log-linear scale. The acoustic impedance $Z_{l=0}$ is equal to Z_w, that of water. As l increases, the real part of Z_l/Z_a falls rapidly, and reaches unity at $l = 0.002\,64\lambda$ (all referenced to the experimental temperature of 25 °C). In contrast, $|\mathrm{Im}[Z_l/Z_a]|$ rises rapidly to a value of 1820 before gradually decreasing to 60.3 when $l = 0.002\,64\lambda$. We exploit this behavior in the design of what essentially is a metasurface-based impedance transformer.

According to Eq. (1), there are no reflected waves when $l = 0.002\,64\lambda$, in which case $\mathrm{Im}[Z_l]$ vanishes. To this end, consider canceling the effectively capacitive imaginary component of Eq. (2) by the insertion of a suitable inductive component. In acoustics, the impedance of a sliding mass with no friction is inductive [61]. If we insert a localized mass m at the virtual interface, as shown in Fig. 1(c), thus forming a mass-cavity metamaterial element, the quantity Z_l in Eq. (2) is modified to

$$Z_l' = \frac{Z_w}{1 + (Z_w^2/Z_a^2 - 1)\sin^2(2\pi \frac{l}{\lambda})} + j\left(\frac{2\pi c_a}{\lambda}\frac{m}{S^2} - \frac{Z_a}{2}\frac{(Z_w^2/Z_a^2 - 1)\sin(4\pi \frac{l}{\lambda})}{1 + (Z_w^2/Z_a^2 - 1)\sin^2(2\pi \frac{l}{\lambda})} \right). \tag{3}$$

The acoustic impedance Z_l' is approximately equal to Z_a under the following conditions

$$l = \frac{c_a}{\omega\sqrt{Z_w/Z_a + 1}} \approx 0.002\,64\lambda \tag{4}$$

and

$$m = \frac{S^2 Z_a}{\omega}\left(1 - \frac{Z_a}{Z_w}\right)\sqrt{\frac{Z_w}{Z_a} + 1} \approx 9.60\lambda\rho_a S, \tag{5}$$

where ω is the angular frequency of the incident wave. Plots of $|\mathrm{Re}[Z_l'/Z_a]|$ and $|\mathrm{Im}[Z_l'/Z_a]|$ vs l/λ under the second condition [Eq. (5)] are shown in Fig. 1(d). The impedance of water is thus transformed to that of air by inserting the mass-cavity element that satisfies two conditions, i.e., Eqs. (4) and (5), at the air-water interface. However, in practice, such a frictionless element is not easily realizable. We therefore adopt an approach based on membrane metamaterials [49–54,62,63]. Such studies have shown that one can

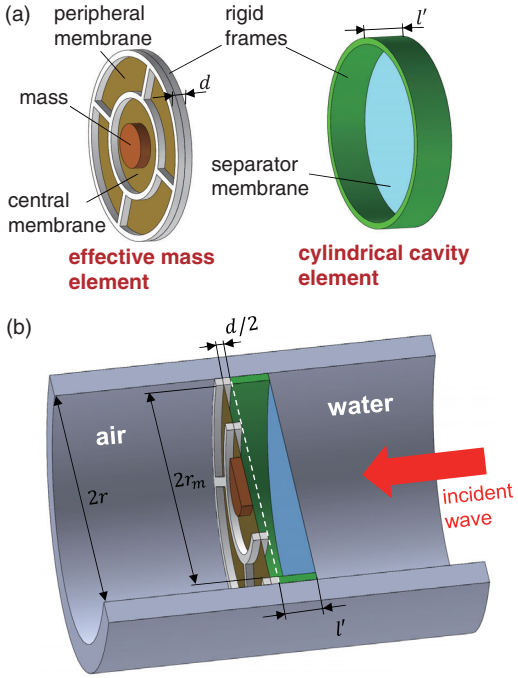

FIG. 2. (a) Structure of the meta-atom, shown in exploded view, composed of an effective mass element and a cylindrical cavity element. (b) Diagram of the meta-atom installed in the waveguide, with acoustic incidence from the water side.

achieve a large effective mass with low losses by use of an appropriate membrane resonance.

Figures 2(a) and 2(b) show our proposed meta-atom for impedance matching, incorporating a membrane-based effective mass to achieve the required inductive effect and also a cylindrical cavity element. Hybrid resonances of a single membrane with a loaded mass have previously been studied for efficient sound absorption [46]. Our design of effective mass element is different, consisting of a central membrane with a mass at the center and four separate peripheral membranes. The number of peripheral membranes is not important: even a single ring-shaped membrane would suffice, but in this case it would be difficult to realize. The proposed structure relies on a simple resonant mode of the structure. The cylindrical cavity element is terminated by a circular separator membrane to prevent water entering the cavity and to allow the volume of the cavity to be accurately controlled.

All the membranes of the effective mass element are made of stretched latex rubber of thickness 57 μm, and are fixed to a rigid aluminium-alloy frame. The outer radius of the peripheral membranes and the radius of the element are $r_m = 12$ mm and $r = 15$ mm, respectively. The inner radius of the peripheral membranes is 8.5 mm and the radius of the central membrane is 6 mm. The latter contains an attached 60 mg epoxy mass of radius 3.5 mm. The total thickness d of the element is 4.1 mm (Further details of the geometry are given in the Supplemental Material [16].). The effective mass element has acoustic impedance $j\omega m_{\rm eff}/S_m^2$, where $S_m = \pi r_m^2$ and $m_{\rm eff}$ is the effective mass. Equation (5) implies $j\omega m/S^2 = 60.3 Z_a j$. As shown in the Supplemental Material [16], the acoustic impedance gradually changes from $-0.856 Z_a j$ to $96.0 Z_a j$ as the frequency is changed from 560 to 750 Hz, taking the value $60.3 Z_a j$ at 707 Hz.

The cylindrical cavity element is formed from a ring-type rigid frame made of acrylonitrile butadiene styrene, in which a thin polyethylene separator membrane of thickness 10 μm and radius $r_m = 12$ mm is fixed. (The acoustic impedance of this membrane is negligibly small compared to that of water.) To choose the cavity length l', the impedance matching conditions (4) and (5) need to be modified to account for $r_m < r$ and the volume next to each membrane. The modified conditions, derived in the Supplemental Material [16], are

$$V_c = \frac{S_m c_a}{\omega}\sqrt{\frac{Z_w/Z_a - 1}{\beta^2 Z_w^2/Z_a^2 - 1}}\left\{1 + \frac{b_{\rm cav} - \omega {\rm Im}[m_{\rm eff}]}{2 Z_a S_m^2 (1 - Z_a/Z_w)}\right\} \quad (6)$$

and

$$\begin{aligned}\frac{{\rm Re}[m_{\rm eff}]}{S_m^2} &= \frac{Z_a}{\omega}\sqrt{\frac{Z_w}{Z_a} - 1}\sqrt{1 - \frac{1}{\beta^2}\frac{Z_a^2}{Z_w^2}} \\ &\quad \times \left\{1 - \frac{(b_{\rm cav} - \omega {\rm Im}[m_{\rm eff}])(1 - 2Z_a/Z_w)}{2 Z_a S_m^2 (1 - Z_a/Z_w)}\right\} \\ &\approx \frac{60.3 Z_a}{\omega}\left(1 - \frac{b_{\rm cav} - \omega {\rm Im}[m_{\rm eff}]}{2 Z_a S_m^2}\right), \end{aligned} \quad (7)$$

where $\beta = S_m/S$, $V_c = S_m l' + V'$, $S_m l'$ is the air volume in the cylindrical cavity element ($V' = 6.09 \times 10^{-7}$ m^3 is the extra air volume occupied by the five cavities formed between the membranes and the plane defining the interface between the effective mass element and the cylindrical cavity element), and $b_{\rm cav}$ is a real damping coefficient to take account of losses in the cavity. A rigorous analysis of such losses could be carried out using fluid dynamics [64]. However, one can use an equivalent electrical transmission line model [65], in which cavity dissipation can be represented by an electrical resistance ($= b_{\rm cav}/S_m^2$) for the special case in which $d/2 + l' \ll \lambda$, obtainable by fitting. The modified conditions (6) and (7) are a reasonable approximation in the dissipative case. As shown in the Supplemental Material [16], ${\rm Im}[m_{\rm eff}]$ arises from dissipation. The required damping coefficients for the effective mass element could again in principle be calculated using fluid dynamics [59,61,64–66]. However, these coefficients can be obtained by fitting. The cavity length $l' = 0.671$ mm (corresponding to $V_c = 9.13 \times 10^{-7}$ m^3) is chosen by use of Eqs. (6) and (7) for the lossless case ($b_{\rm cav} = 0$ and ${\rm Im}[m_{\rm eff}] = 0$), which provides a reasonable first approximation.

The transmission loss spectra of the meta-atom in the waveguide represented in Fig. 2(b) are measured in

experiment and evaluated by finite element modeling (FEM—we make use of the solid mechanics module, the membrane module, and the thermoviscous acoustics module, including viscosity, in COMSOL 5.2a assuming an isothermal boundary [16]). The acoustic wave is incident from the water side, and all the parameters of the meta-atom are as before. In the simulation (with a rigid membrane frame), the dissipation is assumed to be viscothermal, i.e., a combination of the viscous and heat conduction losses of air and water. The central and peripheral membrane tensions are chosen as 67.5 and 44.4 N/m to match the experimental resonance. The transmission loss spectra in the presence of the meta-atom are shown in Fig. 3(a) by the solid blue line (FEM) and dotted blue line (experiment), indicating a minimum of 5.6 dB at 705 Hz. The experimental results are in broad agreement with the trends of the FEM results. In contrast, if the meta-atom is not installed, we obtain the data indicated by the dashed red line (FEM) and the red triangles (experiment). At 705 Hz, the meta-atom increases the power transmission by a factor of 160 to a value of ∼30%, equivalent to a 22 dB enhancement. This remarkable increase is achieved with a meta-atom of thickness $l'+d=$ 4.8 mm that corresponds to the extremely small value $\sim\lambda/100$ in air. (The wavelengths in air and water are, respectively, estimated as 491 and 2120 mm at 705 Hz.)

The power transmission (τ) and reflection (R) coefficients based on the analytical model are derived in the Supplemental Material [16] in the form

$$\tau=\frac{4Z_w/Z_a}{\{(\frac{Z_w}{Z_a}+1)\cos[\frac{\omega V_c}{S_m c_a}]-\frac{\omega}{Z_a}\frac{M'_{\rm eff}}{S_m^2}\frac{Z_w}{Z_a}\beta\sin[\frac{\omega V_c}{S_m c_a}]\}^2+\{(\frac{Z_w}{Z_a}\beta+\frac{1}{\beta})\sin[\frac{\omega V_c}{S_m c_a}]+\frac{\omega}{Z_a}\frac{M'_{\rm eff}}{S_m^2}\cos[\frac{\omega V_c}{S_m c_a}]\}^2}, \tag{8}$$

and

$$R=\frac{\{(\frac{Z_w}{Z_a}-1)\cos[\frac{\omega V_c}{S_m c_a}]-\frac{\omega}{Z_a}\frac{M'_{\rm eff}}{S_m^2}\frac{Z_w}{Z_a}\beta\sin[\frac{\omega V_c}{S_m c_a}]\}^2+\{(\frac{1}{\beta}-\frac{Z_w}{Z_a}\beta)\sin[\frac{\omega V_c}{S_m c_a}]+\frac{\omega}{Z_a}\frac{M'_{\rm eff}}{S_m^2}\cos[\frac{\omega V_c}{S_m c_a}]\}^2}{\{(\frac{Z_w}{Z_a}+1)\cos[\frac{\omega V_c}{S_m c_a}]-\frac{\omega}{Z_a}\frac{M'_{\rm eff}}{S_m^2}\frac{Z_w}{Z_a}\beta\sin[\frac{\omega V_c}{S_m c_a}]\}^2+\{(\frac{1}{\beta}+\frac{Z_w}{Z_a}\beta)\sin[\frac{\omega V_c}{S_m c_a}]+\frac{\omega}{Z_a}\frac{M'_{\rm eff}}{S_m^2}\cos[\frac{\omega V_c}{S_m c_a}]\}^2}. \tag{9}$$

The complex constant $M'_{\rm eff}$ is defined as

$$M'_{\rm eff}\equiv m_{\rm eff}-j\frac{b_{\rm cav}}{\omega}, \tag{10}$$

where the effective mass $m_{\rm eff}$ can be expressed as

$$m_{\rm eff}=\frac{M_c M_p}{M_c+M_p}S_m^2. \tag{11}$$

Here, $M_c\equiv m_c[(1-\omega_c^2/\omega^2)-jb_c/\omega m_c]/S_c^2$ and $M_p\equiv m_p[(1-\omega_p^2/\omega^2)-jb_p/\omega m_p]/S_p^2$. The central-membrane area S_c is 0.000 11 m^2, and the peripheral membrane total area S_p is 0.000 18 m^2. The quantities ω_c, ω_p are the resonance frequencies of the central and peripheral membranes, respectively. The related coefficients b_c and b_p depend on the dissipation [59–61]; the corresponding loaded masses, given by m_c and m_p, include the effect of the inertances of the associated air columns [61]. The values $f_c=\omega_c/2\pi=562$ Hz, $f_p=\omega_p/2\pi=4671$ Hz, $m_c=0.171$ g, $m_p=0.009\,90$ g, $b_c=0.002\,00$ kg/s, $b_p=0.000\,960$ kg/s, and $b_{\rm cav}=0.104$ kg/s are extracted by least-squares fitting to experiment, whereas other parameters of the meta-atom are taken from the experimental realization.

We plot in Fig. 3(b) the experimental, analytical, and FEM results for power transmission (τ) and reflection (R) and in Fig. 3(c) the dissipated power ratio (dissipated power divided by the incident power). In Fig. 3(c) the results of FEM are shown as follows: the total dissipation is represented by the black dotted line and is made up of the sum of the heat conduction losses (red triangles) and viscous losses (dashed green line); the heat conduction losses make up 84% of the total dissipation. The analytical curves for τ, R, and dissipated power lie almost on the FEM curves. The experimental results are in broad agreement with the trends of these curves, but show slightly larger bandwidth. (The exact origin of these residual deviations is difficult to speculate on. Some negative values of dissipated power ratio in Fig. 3(c) arise from experimental noise.) However, in all cases, on resonance about 1/3 of the power is transmitted, 1/3 is reflected, and the rest is dissipated. Some reflection is inevitable considering that l' was chosen according to Eq. (6) under the idealized condition $b_{\rm cav}=0$. (In the Supplementary Material [16], we show that the meta-atom allows almost perfect impedance matching at 707 Hz in this case.) In the simulations, we have assumed that the viscoelastic and thermoelastic losses in the membranes are negligible compared to viscothermal losses. The reasonable agreement between the analytical model (which includes general losses) and the simulation (which only includes viscothermal losses) in Fig. 3 supports this assumption. Calculations of the dissipation in the cavity by FEM point to this as being the dominant region for these viscothermal losses.

In practical applications, such as air-to-water communication or vice versa, one should use a 2D array of meta-

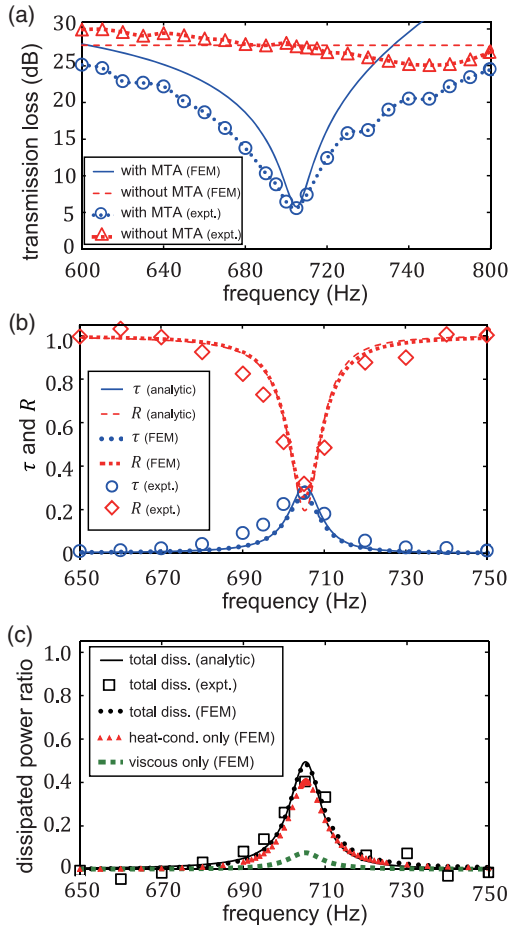

FIG. 3. (a) Experimental and FEM transmission loss from water to air vs frequency. Dotted blue line (experiment) and solid blue line (FEM): case with the meta-atom. Red triangles (experiment) and dashed red line (FEM): case without meta-atom. (b) Experimental (blue circles), FEM (blue dotted line), and analytical (blue solid line) power transmission (τ) from water to air vs frequency and corresponding plots for power reflection coefficient (R) (see legend). In FEM for (a) and (b), dissipation arising from the viscosities and heat conduction of air and water are included. In the analytical calculations, dissipation is included by fitting. (c) Experimental (black squares), FEM (black dotted line), and analytical (black solid line) total dissipated power ratio (dissipated power divided by the incident power) vs frequency. Also plotted is the contribution to the dissipated power ratio by heat conduction losses (red triangles) and by viscous losses (dashed green line). (Meta-atom, MTA; dissipation, diss.)

atoms to form a metasurface. In contrast to the single meta-atom case held by a rigid support, the center-of-mass vibration of the frame should no longer be ignored. However, this does not prevent an excellent value of transmission from being obtained, although one can show that the matching frequency is increased owing to the frame and membrane vibrations about the center of the mass [16].

In conclusion, we demonstrate experimentally, theoretically, and by simulation a meta-atom that works as an acoustic impedance transformer between air and water in spite of their huge impedance mismatch. With a meta-atom thickness of only $\sim\lambda/100$, we measure a transmission loss of 5.6 dB, corresponding to an intensity transmission 160 times that of a bare air-water interface. One could improve this on-resonance transmission by new designs with, for example, a reduced surface-to-volume ratio of the cavity. We also show that a 2D array of these meta-atoms forms an impedance matching metasurface, which should prove invaluable for practical devices. The metasurface can be tuned by, for example, modifying the membrane tension or the cavity length, and should therefore be very versatile for the efficient reception of audio sound or ultrasonic waves in air from underwater sources or in water from airborne sources.

This work was supported by the Center for Advanced Meta-Materials (CAMM) funded by the Ministry of Science, ICT, and Future Planning as a Global Frontier Project (CAMM-2014M3A6B3063712) and by the National Research Foundation of Korea(NRF) Grant funded by the Korea government (MSIP) (No. 2015001948).

*samlee@yonsei.ac.kr

[1] M. La Mura, N. A. Lamberti, B. L. Mauti, G. Caliano, and A. S. Savoia, Ultrasonics **73**, 130 (2017).
[2] H. Fang, Y. Chen, C. Wong, W. Qiu, H. Chan, J. Dai, Q. Li, and Q. Yan, Ultrasonics **70**, 29 (2016).
[3] J. A. Brown, S. Sharma, J. Leadbetter, S. Cochran, and R. Adamson, IEEE Trans. Ultrason. Ferroelectr. Freq. Control **61**, 1911 (2014).
[4] G.-H. Feng and W.-F. Liu, Sensors **13**, 13543 (2013).
[5] Y. Li, J. Tu, B. Liang, X. Guo, D. Zhang, and J. Cheng, J. Appl. Phys. **112**, 064504 (2012).
[6] Q. Zhou, J. H. Cha, Y. Huang, R. Zhang, W. Cao, and K. K. Shung, IEEE Trans. Ultrason. Ferroelectr. Freq. Control **56**, 213 (2009).
[7] T. G. Álvarez-Arenas, IEEE Trans. Ultrason. Ferroelectr. Freq. Control **51**, 624 (2004).
[8] D. Callens, C. Bruneel, and J. Assaad, NDT&E Int. **37**, 591 (2004).
[9] M. Toda, IEEE Trans. Ultrason. Ferroelectr. Freq. Control **49**, 299 (2002).
[10] H. Persson and C. Hertz, Ultrasonics **23**, 83 (1985).
[11] H. Zhang, Z. Wei, L. Fan, J. Qu, and S. Zhang, Sci. Rep. **6**, 34688 (2016).
[12] B. E. McDonald and D. C. Calvo, J. Acoust. Soc. Am. **122**, 3159 (2007).
[13] O. A. Godin, Phys. Rev. Lett. **97**, 164301 (2006).
[14] V. W. Sparrow, J. Acoust. Soc. Am. **111**, 537 (2002).
[15] R. A. Sohn, F. Vernon, J. A. Hildebrand, and S. C. Webb, J. Acoust. Soc. Am. **107**, 3073 (2000).
[16] See Supplemental Material at http://link.aps.org/supplemental/10.1103/PhysRevLett.120.044302 for details of the expected sensitivity enhancement obtained by the use of in-air microphones in conjunction with the metasurface, analysis of the effective mass element including an analytical approach, experimental details and FEM, analytical

calculations of the impedance matching conditions and the transmission and reflection coefficients, and a simulation of a 2D square-lattice array metasurface, which includes Refs. [17–35].
[17] See data sheet B&K hydrophone types 8103, 8104, 8105, and 8106, https://www.bksv.com/-/media/literature/Product-Data/bp0317.ashx.
[18] See data sheet Teledyne RESON hydrophone type TC4013, https://www.m-b-t.com/fileadmin/redakteur/Ozeanographie/Hydrophone/Produktblaetter/TC4013.pdf.
[19] See data sheet Teledyne RESON hydrophone type TC4033, https://www.m-b-t.com/fileadmin/redakteur/Ozeanographie/Hydrophone/Produktblaetter/TC4033.pdf.
[20] See data sheet Teledyne RESON hydrophone type TC4034, https://www.m-b-t.com/fileadmin/redakteur/Ozeanographie/Hydrophone/Produktblaetter/TC4034.pdf.
[21] See data sheet B&K microphone type 4144, https://www.bksv.com/-/media/literature/Product-Data/bp2031.ashx.
[22] See data sheet B&K microphone type 4145, https://www.bksv.com/-/media/literature/Product-Data/bp2032.ashx.
[23] See data sheet B&K microphone type 4958, https://www.bksv.com/-/media/literature/Product-Data/bp2173.ashx.
[24] See data sheet G. R. A. S. microphone type 46AE, https://www.gras.dk/46ae.html.
[25] See data sheet G. R. A. S. microphone type 46AN, https://www.gras.dk/46an.html.
[26] See data sheet G. R. A. S. microphone type 46BL, https://www.gras.dk/46bl.html.
[27] S. H. Lee and O. B. Wright, Phys. Rev. B **93**, 024302 (2016).
[28] S. H. Lee, C. M. Park, Y. M. Seo, Z. G. Wang, and C. K. Kim, Phys. Lett. A **373**, 4464 (2009).
[29] B. H. Song and J. S. Bolton, J. Acoust. Soc. Am. **107**, 1131 (2000).
[30] Material Database in COMSOL MULTIPHYSICS 5.2a.
[31] https://www.matbase.com/material-categories/natural-and-synthetic-polymers/elastomers/material-properties-of-natural-rubber-polyisoprene-ir.html#properties.
[32] http://www.engineeringtoolbox.com/poissons-ratio-d_1224.html.
[33] http://www.mse.mtu.edu/~drjohn/my4150/props.html.
[34] M. Holmes, N. Parker, and M. Povey, J. Phys. Conf. Ser. **269**, 012011 (2011).
[35] http://www.vinidex.com.au/technical/material-properties/polyethylene-properties/.
[36] Z. Li, D. Yang, S. Liu, S. Yu, M. Lu, J. Zhu, S. Zhang, M. Zhu, X. Guo, H. Wu *et al.*, Sci. Rep. **7**, 42863 (2017).
[37] M. Yang, S. Chen, C. Fu, and P. Sheng, Mater. Horiz. **4**, 673 (2017).
[38] G. Ma and P. Sheng, Sci. Adv. **2**, e1501595 (2016).
[39] S. A. Cummer, J. Christensen, and A. Alù, Nat. Rev. Mater. **1**, 16001 (2016).
[40] R. Fleury and A. Alù, J. Acoust. Soc. Am. **136**, 2935 (2014).
[41] S. H. Lee, C. M. Park, Y. M. Seo, Z. G. Wang, and C. K. Kim, Phys. Rev. Lett. **104**, 054301 (2010).
[42] N. Yu, P. Genevet, M. A. Kats, F. Aieta, J.-P. Tetienne, F. Capasso, and Z. Gaburro, Science **334**, 333 (2011).
[43] B. Yuan, Y. Cheng, and X. Liu, Appl. Phys. Express **8**, 027301 (2015).
[44] K. Song, J. Kim, S. Hur, J. Kwak, S. Lee, and T. Kim, Sci. Rep. **6**, 32300 (2016).
[45] N. Jiménez, V. Romero-García, V. Pagneux, and J.-P. Groby, Sci. Rep. **7**, 13595 (2017).
[46] G. Ma, M. Yang, S. Xiao, Z. Yang, and P. Sheng, Nat. Mater. **13**, 873 (2014).
[47] R. Al Jahdali and Y. Wu, Appl. Phys. Lett. **108**, 031902 (2016).
[48] C. Shen, J. Xu, N. X. Fang, and Y. Jing, Phys. Rev. X **4**, 041033 (2014).
[49] G. Ma, M. Yang, Z. Yang, and P. Sheng, Appl. Phys. Lett. **103**, 011903 (2013).
[50] C. J. Naify, C.-M. Chang, G. McKnight, and S. Nutt, J. Appl. Phys. **110**, 124903 (2011).
[51] C. J. Naify, C.-M. Chang, G. McKnight, F. Scheulen, and S. Nutt, J. Appl. Phys. **109**, 104902 (2011).
[52] C. J. Naify, C.-M. Chang, G. McKnight, and S. Nutt, J. Appl. Phys. **108**, 114905 (2010).
[53] Z. Yang, H. Dai, N. Chan, G. Ma, and P. Sheng, Appl. Phys. Lett. **96**, 041906 (2010).
[54] Z. Yang, J. Mei, M. Yang, N. H. Chan, and P. Sheng, Phys. Rev. Lett. **101**, 204301 (2008).
[55] M. Yang, C. Meng, C. Fu, Y. Li, Z. Yang, and P. Sheng, Appl. Phys. Lett. **107**, 104104 (2015).
[56] M. Yang, Y. Li, C. Meng, C. Fu, J. Mei, Z. Yang, and P. Sheng, C.R. Mec. **343**, 635 (2015).
[57] J. Mei, G. Ma, M. Yang, Z. Yang, W. Wen, and P. Sheng, Nat. Commun. **3**, 756 (2012).
[58] A. A. Maznev, A. G. Every, and O. B. Wright, Wave Motion **50**, 776 (2013).
[59] L. E. Kinsler, A. R. Frey, A. B. Coppens, and J. V. Sanders, *Fundamentals of Acoustics* (John Wiley & Sons, New York, 1999).
[60] J. J. Park, K. J. B. Lee, O. B. Wright, M. K. Jung, and S. H. Lee, Phys. Rev. Lett. **110**, 244302 (2013).
[61] D. T. Blackstock, *Fundamentals of Physical Acoustics* (John Wiley & Sons, New York, 2000).
[62] H. Zhang, Y. Xiao, J. Wen, D. Yu, and X. Wen, Appl. Phys. Lett. **108**, 141902 (2016).
[63] Y. Chen, G. Huang, X. Zhou, G. Hu, and C.-T. Sun, J. Acoust. Soc. Am. **136**, 969 (2014).
[64] M. R. Stinson, J. Acoust. Soc. Am. **89**, 550 (1991).
[65] T. L. Szabo, J. Acoust. Soc. Am. **45**, 124 (1969).
[66] J. Pelzl, K. Klein, and O. Nordhaus, Appl. Opt. **21**, 94 (1982).